Towards a novel single-LED pulse oximeter based on a multispectral sensor for IoT applications

Alejandro von Chong, Mehdi Terosiet, Aymeric Histace, Olivier Romain

Journal logo

Towards a Novel Single-LED Pulse Oximeter Based on a Multispectral Sensor for IoT applications

A.Von Chong, M. Terosiet, A. Histace and O. Romain

Laboratoire ETIS - Université Cergy-Pontoise – ENSEA – CNRS, Cergy-Pontoise, France. Mail to : alejandro.von-chong@ensea.fr

Elsevier use only: Received date here; revised date here; accepted date here

Abstract

Pulse oximetry is one of the most commonly employed monitoring modalities in critical care setting. Conventional pulse oximeters use two leds at different wavelengths and a photodiode to estimate blood oxygen saturation noninvasively, based in the difference of absorption coefficients between hemoglobin and deoxyhemoglobin. Nevertheless, factors such as low oxygen saturations or led wavelength displacement, modify differently the expected light absorbance for both LEDs. To address this issue, we propose a novel approach combining a single led and a Buried Quad Junction photodetector, i.e. a multispectral sensor. With this fundamental modification of the pulse oximetry principle, we reduce the modifying effects introduced by the aforementioned sources of inaccuracy by using a single led. Results from in vivo measurements, show that two of the three tests of the proposed system's precision falls within the commercial tolerance of 3% SpO_2%, while for the third, a maximum error of 4% was found.

Keywords : Pulse oximetry; multiwavelength oximetry; BQJ; blood plethysmography;

1. Introduction

Pulse oximeters have become an essential tool for patient monitoring, ranging from intensive care units and operating rooms in hospitals, to sleep disorder supervision in the patient's home. They rely on the photoplethysmography technique for non-invasively estimating the saturation of arterial blood with oxygen (SpO_2). This is a major indicator of a patient's cardio-respiratory status since it provides the percentage of hemoglobin bound with oxygen in the arterial blood. Indeed, for healthy patients, the majority of molecular oxygen (O_2) is bound to hemoglobin and only a small fraction is dissolved in plasma. However, patients suffering from respiratory problems or certain metabolic and genetic disorders, can reach a dangerously low amount of oxygenated hemoglobin [1]. Beyond these applications, additional information other than oxygenation can be derived with the photopleghysmography technique, *i.e.* the plethysmogram waveform (PPG). This additional information include the heart rate, tissue perfusion and arterial stiffness [2].

With classic pulse oximeters, the arterial blood saturation (SpO_2) is estimated with an optical setup

working on well perfused tissue such as a finger or earlobe. This setup is composed of two light emitting diodes (LED), usually red at 660 nm and infrared at 940 nm, alternatively shining through the tissue and, on the opposite side, a detector measures the transmitted light, which was not absorbed by other light absorbents in finger, such as blood, skin, nails and bone, see Fig. 1. These wavelengths are widely used because of the hemoglobin's optical properties: at 660 nm, deoxygenated hemoglobin (deoxyhemoglobin or Hb) absorbs more light than oxygenated hemoglobin (oxyhemoglobin or HbO_2) while at 940 nm, oxyhemoglobin absorbs more light than deoxyhemoglobin. The ratio between the two absorption coefficients is approximately tenfold [3].

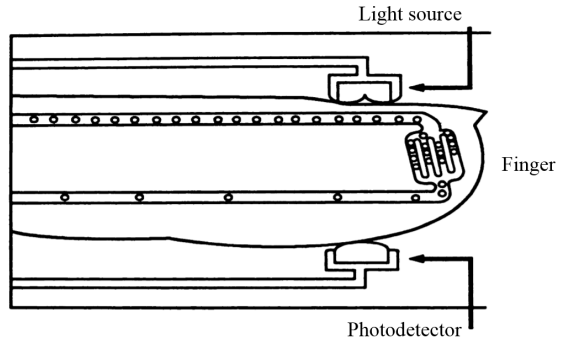

Fig. 1. Optical setup [4].

From there, and with some electronic circuitry, the PPG signals at 660 nm and 940 nm are acquired. Fig. 2 illustrates their typical waveform. The AC/DC ratio of their respective components is blood oxygenation-dependent. The relationship between this AC/DC ratio and SpO_2 is then empirically calibrated [5]. However, this approach exhibits some limitations.

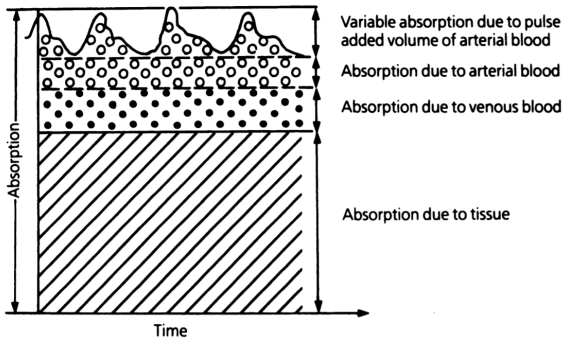

Fig. 2. Typical plethysmograph signal [4].

2. Problem statement

Classical oximeters are subjected to several sources of inaccuracies. The fact is that there are discrepancies in accuracy between commercial pulse oximeters, in part, as a result of the differences in their calibration processes and algorithms employed for their signal processing. One of them is observed when oxygen saturation drops below 70%, the scattering difference between these two wavelengths affect the SpO_2 estimation [6]. Calibration-free pulse oximetry addresses this problematic, but its practical implementation still poses some technological limitations [7]. Another important source of erroneousness is related to the wavelength displacement of the incident wave from its typical value. A led's peak emission wavelength might be shifted due to a change in the led's temperature, ageing or fabrication processes. A change of just 4 nm in one of the led's peak emission (with the other led's peak emission wavelength remaining constant) produces an error of 2% at 97% SpO_2, 4% at 90% SpO_2 and 7% at 80% SpO_2 [8].

Considering these limitations, recently manufactured oximeters use up to 8 wavelengths to improve accuracy, increase performance at low saturations and enhance robustness against noise and motion artifacts. Moreover, the wavelength addition enables the estimation of other types of hemoglobins such as carboxyhemoglobin and methemoglobin. This is the case for the Masimo SET® pulse co-oximeters very often used as gold-standards in literature [9, 10, 11].

In the field of Internet-of-Things for biomedical applications, almost everything remains to be done as regards to these last considerations. Even if a remarkable work was published by Theodor *et al.*, in [12], with a pulse oximeter implanted in subcutaneous tissues, the deviations of their results are above the accepted limit range defined by the ISO 80601-2-61 standard [8]. Another work, in accordance with the paradigm of N-wavelength oximetry (N=1, 2, 3, ...), show a real interest for connected wearable pulse oximeters [13]. This study examines the possibility to design a multi-wavelength LED by using rare-earth excited by a commercial blue LED. On this basis, the authors aim to evaluate a pulse oximeter embedded in a Valencell earbud. However, there is not enough results to conclude. Hence, at this stage, the open-

ended question remains while the direct implementation of an N-LED system runs completely counter to the system miniaturization needed for connected objects.

In this study, we address the emphasized lack of actual devices. For that, we introduce a new paradigm for the instrumentation by substituting the multi-wavelength light source and its associated photodetector by a multi-spectral optical sensor and a single LED. This approach could reduce most of the imprecisions related to the scattering phenomena, and led deterioration. Furthermore, in the perspective of a silicon implementation, it could significantly alleviate the electrical power consumption of the pulse oximeter.

This original idea is laid out into the six following parts. Firstly, the Buried Quad Junction photodetector (BQJ), which is the substrate of the proposed approach is described. Once these elements of understanding are provided, the fundamentals of the new sensing method is given in the fourth section. The experimental setup comprising the electronic acquisition circuit associated to its driving software and the testing protocol are depicted, in the fifth section. Finally, before discussion, conclusion and future perspectives of this work, the experimental proof of concept is provided in the sixth part.

3. Buried Quad Junction – BQJ – Photodetector

Connected devices take advantages of advances in CMOS technology fabrication process. Downscaling has allowed embedding more and more electronic functionalities and the maturity of fabrication process enables the integration of MEMS elements (Micro-Electro-Mechanical Systems) for actuators and sensors [14]. There is now the possibility to design multiple buried-junction photodetectors for applications requiring spectral analysis. The operation of these optical sensors draws on the strong dependence of silicon absorption depth on the incident light wavelength. The exponential decrease in depth of generated photo-carriers is distinctly related to the wavelength. A first CMOS design including two junctions was introduced in 1996 with [15] and was the subject to several studies [16, 17]. One year later, a BiCMOS implementation stacking three buried junctions was presented for colour detection like the previous one [18]. To achieve an highest spectral discrimination ability, authors of these research works have gone one step further and are now proposing the BQJ (Buried Quad Junction) photodetector for which important characterization efforts can be found in [19, 20].

This last upgrade is designed by Teledyne-DALSA with a 0.8 µm High Voltage CMOS process. As depicted by Fig. 3, for 200 µm square area, it implements four vertically-stacked p-n junctions with four different spectral responses sensing from near UV to near IR. We take advantage of this particular feature for the single-LED pulse oximeter implementation.

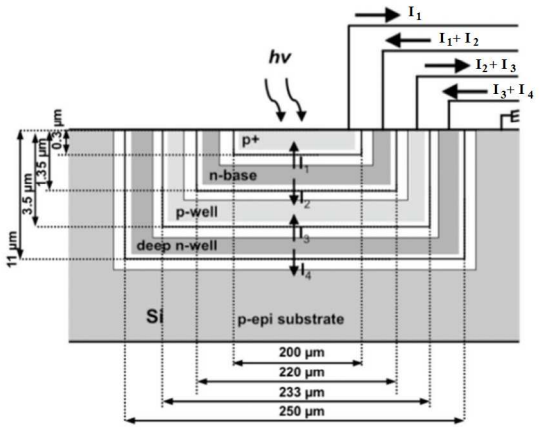

Fig. 3. Sectional view of the BQJ [21].

Each junction drives an output current proportional to the incident light intensity while the normalized current distribution over the four junctions, as a function of the wavelength, is depicted on Fig. 4. This characterization was obtained by measuring current outputs when the sensor was illuminated by a SPEX 270M monochromator.

It is worth noting that, for a given wavelength, a specific and unique current distribution through the four channels is exhibited by the BQJ. By extension, the BQJ's response to an incident light beam, necessarily respects a specific distribution of output currents in accordance with the Fig. 4. The concept to be understood for the next section is: a light beam, with a specific optical spectrum, implies a corresponding signature and thus can be seen as an "equivalent wavelength" from the BQJ's perspective.

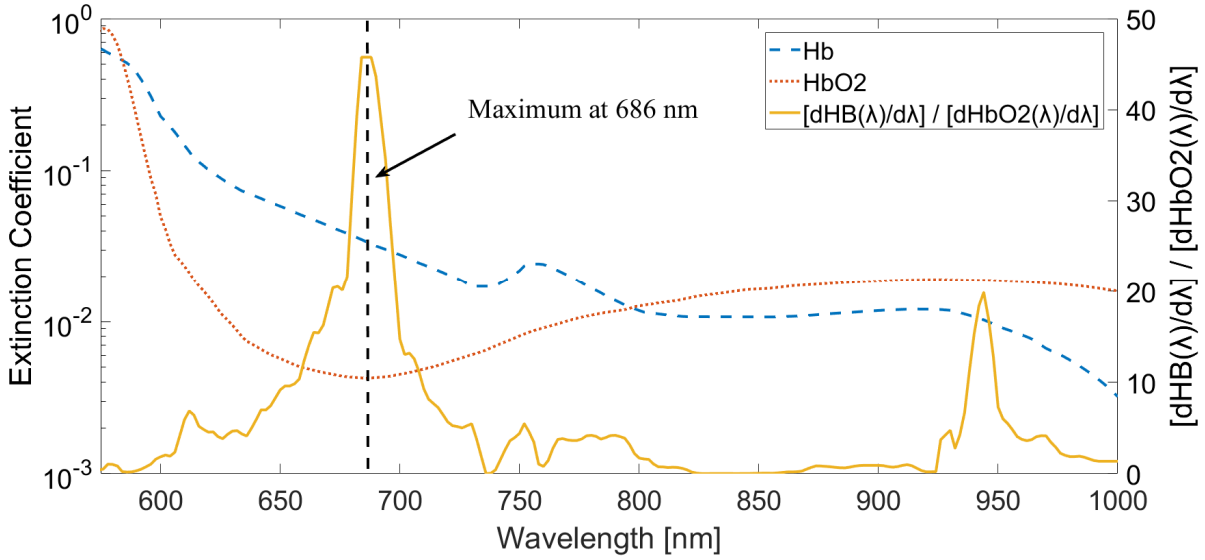

Fig. 5. Left: Oxyhemoglobin (HbO2) and deoxyhemoglobin (Hb) extinction coefficients with respect to the wavelength. Data obtained from [22]. Right: Absolute value of the ratio of the Hb and HbO2 derivatives with respect to wavelength.

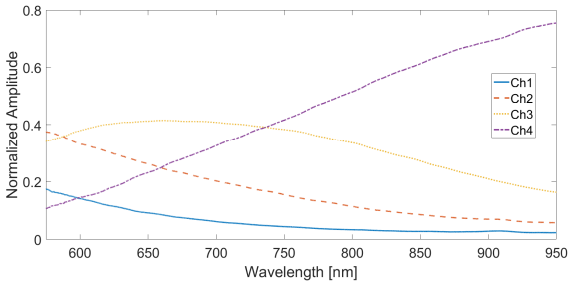

Fig. 4. Normalized response of the BQJ output currents as a function to the wavelength.

By exploiting these unique properties, a novel sensing method was developed. It benefits from the spectral discrimination ability of this compact and smart sensor so as to estimate the blood oxygenation.

4. New sensing approach

4.1. Blood signature extract from the BQJ responses

The optical spectrum of the light transmitted through the finger depends, on one hand, on the light source's spectrum and on the other hand, on the extinction coefficient of blood. Both parameters directly influence the light intensity and spectrum received by the photodetector. Concerning the blood light absorption, the Fig. 5 illustrates its absorption functions related to oxyhemoglobin (HbO_2) and deoxyhemoglobin (Hb) with respect to wavelength.

Oxygenated and deoxygenated blood have different absorption spectrums, meaning that a change in the oxygenation level applies a different optical filter to the led's incident light. So, due to the fact that the BQJ can distinguish changes in the incident's light spectrum, we can use it in order to detect a change of a led's incident light spectrum as blood's oxygenation levels change. The most important change would be seen where there's the biggest slope difference for the two hemoglobin types. In order to determine the best possible wavelength range to exploit this, the derivative of the oxyhemoglobin's and deoxyhemoglobin's absorption spectrum was calculated. The absolute value of the ratio between these derivatives ($[dHb(\lambda)/d\lambda]$ / $[dHbO_2(\lambda)/d\lambda]$) is shown in Fig. 5.

Thus, for the proposed approach, one can see that the range from 660 nm to 700 nm has the biggest slope difference. Due to the commercial availability, a 680 nm (with a spectral line half width of 30 nm) was chosen.

We can conclude that for each SpO_2 value, a signature or a distribution of BQJ's currents is

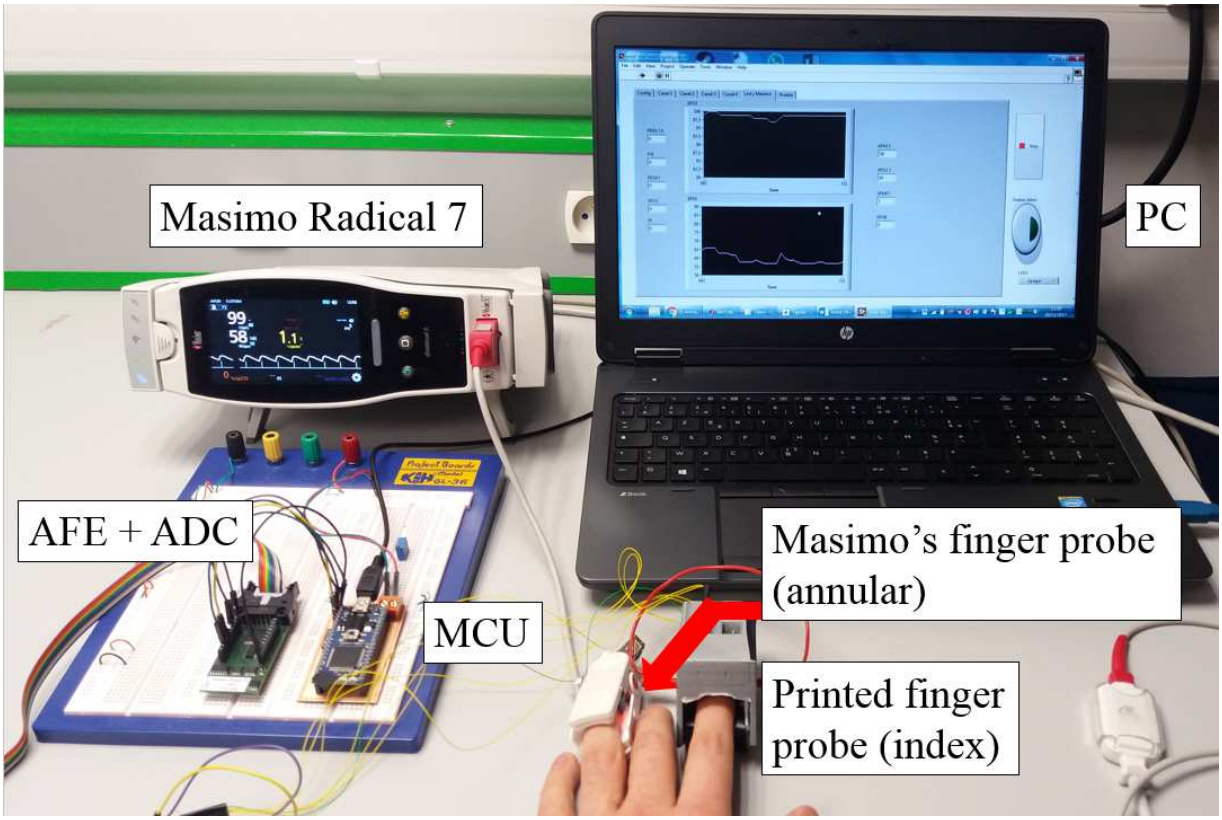

Fig. 6. Measuring setup comprised by the Masimo Radical 7 as the measuring reference, the analog front end, the printed finger probe, the Masimo's Radical 7 finger probe and the PC with the LabVIEW-based acquisition software.

associated. Their relation depends on the signature and their sensitivity slopes where at 680 nm the contrast is enhanced between oxygenated and deoxygenated blood. What differentiates this method from the classic approach, is that the latter measures the change in absorbance for two different wavelengths, while we measure the spectral change for a single wavelength using a multispectral photodetector.

4.2. Arterial saturation estimation

For the arterial oxygen saturation estimation, we use the AC amplitudes of the resulting PPG. Remembering that the BQJ's output currents are proportional to light intensity and that, for a specific wavelength, current distribution remains constant, we calculate a ratio between channels which we denote by $\beta_{i,j}$ as in equation 1.

$$\beta_{i,j} = \frac{AC_{chi}}{AC_{chj}} \quad (1)$$

Where $AC_{ch\,i,j}$ stand for the AC output of the resulting plethysmogram for two different channels. Thus, an estimation of the oxygen saturation can be made by using one led.

In our case, the normalization of the DC components is not necessary in order to nullify the difference in intensities because the magnitude of all outputs are already linearly dependent.

5. Experimental Setup

So as to validate the proposed approach and the sensing method, we developed an acquisition system which associates mixed electronic circuits and its driving software shown in Fig. 6.

5.1. Hardware setup

5.1.1. Acquisition system

The acquisition system is illustrated in Fig. 7. BQJ's output currents pass through signal conditioning circuit in order to obtain voltages of resulting from the received beam light. These voltages are acquired by the 24 bit ΣΔ Analog-to-Digital converter ADS1220. Digital data are then read by a LPC1768 microcontroller (32-bits ARM Cortex-M3) and sent to a host computer using LabVIEW for monitoring and data storage in spreadsheet files. The Masimo Radical 7 was used as the measuring reference and data were recorded simultaneously with the ADC measurements by the host computer.

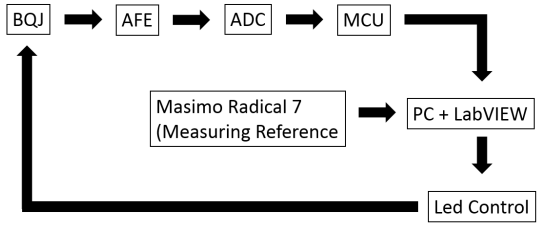

Fig. 7. Block diagram of the utilized system

5.1.2. Signal conditioning circuitry

The AFE is designed in order to process BQJ's output currents, see Fig. 8. These outputs are converted from current to voltage with a Transimpedance-Amplifier built from an OPA4348 (Texas Instruments, 4 channel - single supply). A second order low-pass filter is set at a cut-off frequency of 10 Hz because all the useful information is contained within the 0-10 Hz band. An instrumentation amplifier, with INA2332 (Texas Instruments, CMRR 73 dB), is used to subtract the bias voltage, needed for the polarization of each of the BQJ's junctions, and to amplify this voltage difference by 5. The obtained measurements of received light are then digitized by an ADS1220. Finally, the described analog chain is implemented for each channel of the BQJ.

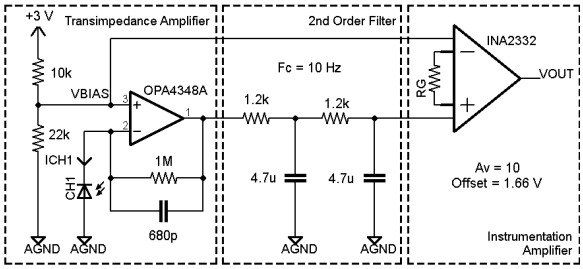

Fig. 8 a. Signal conditioning circuit schematic for each channel.

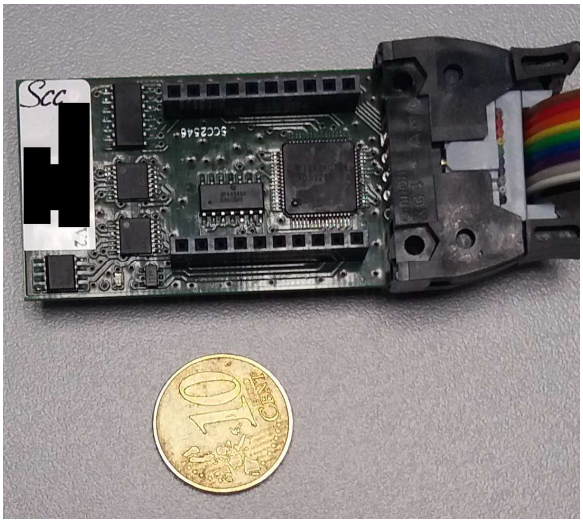

Fig. 8 b. Signal conditioning circuit.

5.1.3. Light Source

The LED selected for this study is the MTE6800N2-UR, Marktech Optoelectronics, which has its peak emission at 681 nm. Its measured optical spectrum is given in Fig. 9

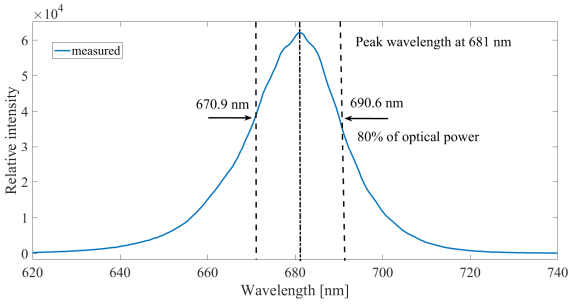

Fig. 9. Measured optical spectrum of the 681 nm, MTE6800N2-UR, Marktech Optoelectronics.

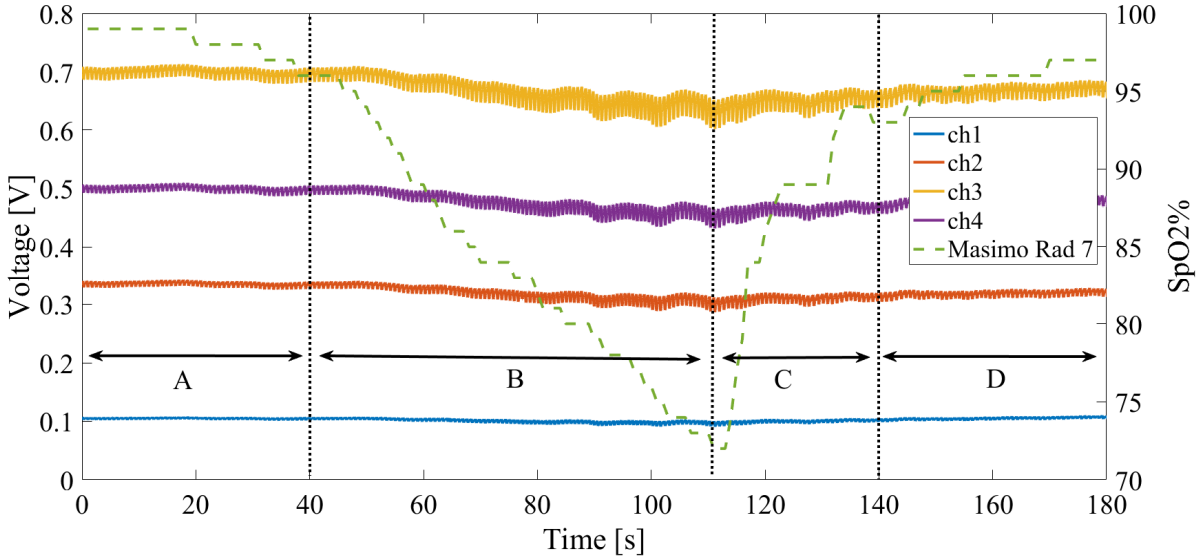

Fig. 10 a. Signals digitized by the ADS1220 with temporal delimitations during the test. Region A represents the relatively constant oxygenation at the beginning the breath holding period. B represents the deoxygenation due to breath holding. C represents the oxygenation due to breathing and D represents the return to the normal oxygenation level.

The spectrophotometric measurements were made with the Avantes AvaSpec-ULS2048L spectrometer for a LED forward current of 5 mA.

In order to hold the BQJ in position, a 3D printed finger probe was produced. The probe held the BQJ in one side and the leds in the opposite side. Careful attention was paid in order to align led beam with the BQJ. The probe had a compression spring in the rear end order to apply a constant pressure to the finger during tests. Silicone was applied to the surface in contact with the finger better contact and comfort. The probe can be seen in Fig. 11.

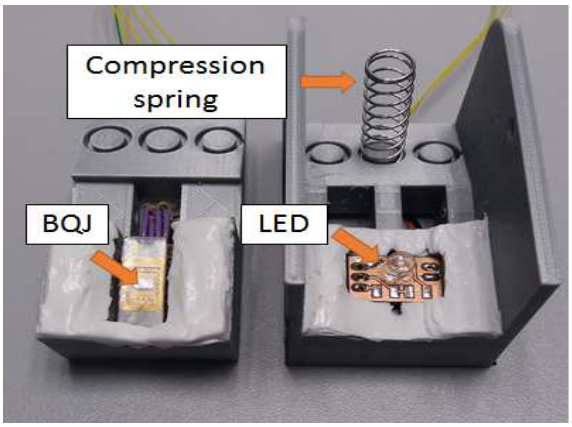

Fig. 11. Printed finger probe.

5.2. Testing Protocol

Measurements were done on 3 subjects by breath holding so as to stop their oxygen supply and thus decreasing their SpO_2. Test were performed in a dark room. Subjects had their arms placed flat on a table at the height of their chests and performed the following protocol:

1. Deep breathing (hyperventilation) during 1 minute.
2. Breath holding.

2.1 Simultaneously with 2, begin data recording.

3. Subject breathes.
4. Continue to record data 1 minute after breathing.
5. Led turn-off (for offset calibration).
6. End test.

Measurements for our system and the reference instrument, the Masimo Radical-7, were made with the left hand: index for our system and annular for the Masimo. For all tests performed, led intensity was unchanged.

6. *In vivo* Results

In order to test our led choice, we performed a first breath holding test with a volunteer for 3 different wavelengths. So as to determine which wavelength was more sensitive to the deoxygenation process through the whole finger (including venous blood), measurements were taken and a Matlab's peak detection algorithm was used. The ratio between peaks and valleys for each channel was calculated. Fig. 12. shows the ratio between channels 3 and 4 for the calculation done previously. Chosen leds had peak wavelengths and spectral line half widths at 640 ± 25 nm, 660 ± 25 nm and 680 ± 30 nm.

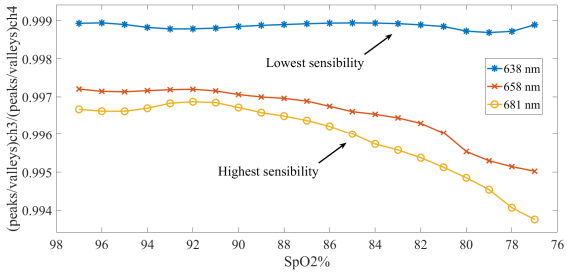

Fig. 12. Sensibility curves for different wavelengths

This way we can conclude that our choice for a 680 ± 30 nm is the appropriate for this application.

From the acquisition system described previously and following the developed protocol, we present in Fig. 10 a sample of the acquired data from a subject and for the four channels of the BQJ.

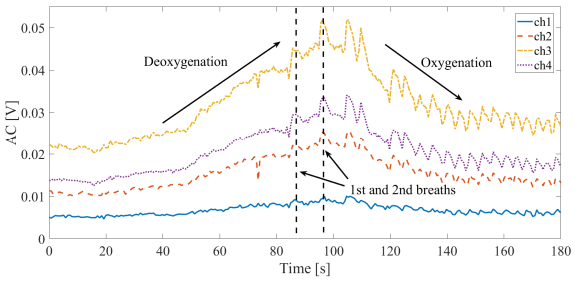

Fig. 13. AC magnitudes obtained for the four channels from the peak detection algorithm.

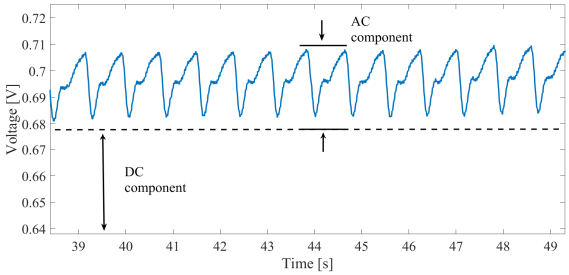

Fig. 10.b. Zoomed output from channel 3 showing plethysmogram with its AC and DC components.

Spreadsheet files containing acquired data were processed afterwards with Matlab where an algorithm for peak detection was used to extract the AC envelope.

After extraction of the peak's and valley's envelope, the AC is calculated by subtracting the former from the latter, results can be seen in Fig. 13.

In order to determine which channels are more sensitive to the spectral change due to the filter applied by the deoxygenation process for the arterial blood, we proceed to calculate the normalized responses of the AC voltages from Fig. 13. This represents the spectral 'signature' seen by the BQJ for the arterial blood. Filtered results are shown in Fig. 14.

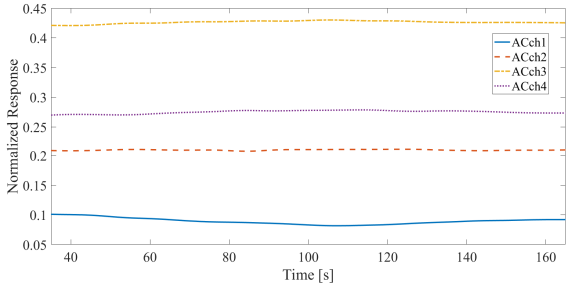

Fig. 14 a. Voltage distribution for the AC components of the PPG.

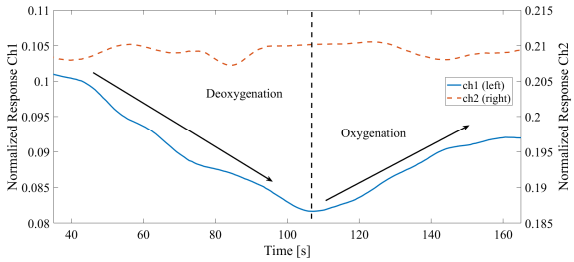

Fig. 14 b. Zoomed voltage distribution during oxygenation and deoxygenation for channels 1 and 2.

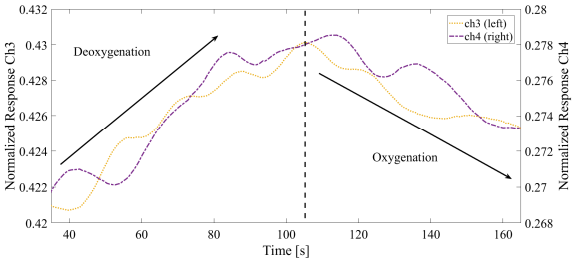

Fig. 14 c. Zoomed voltage distribution during oxygenation and deoxygenation for channels 3 and 4.

As expected, the sensibility changes and the ratio can decrease or increase depending on the chosen channels. Even though channels 3 and 4 are of the same form, we privileged channel 4 because of the higher linearity for a change in wavelength as seen in Fig. 4.

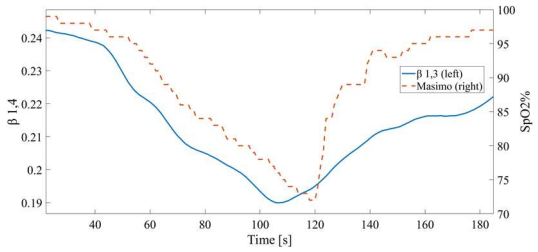

Fig. 15. β between channels 1 and 4 as a function of time.

From there, the relation between the SpO_2 measured by the reference instrument and $\beta_{1,4}$ can be established.

To do so, only the deoxygenation segment of Fig. 15 is considered, because during the breath holding tests, once the volunteer starts to breathe, signals are contaminated by motion artifacts, irregular respiration patterns and abrupt changes in heart rate who decrease the performance of the peak detection algorithm. Curves obtained by breath holding experiment with the three test subjects yielded different oxygenation levels. For comparison purposes, measurement results were truncated to the SpO_2 range shared by the three subjects: 97% to 80% SpO_2.

Finally, Fig. 16 demonstrates the good agreement for the SpO_2 measurements with the three subjects. The commercial permissive tolerance established by the ISO 80601-2-61 standard is 3%. Two of the three tests fall below the tolerated error for the whole process, while the third one, goes above slightly at high saturation (4% error) as seen in Fig. 15b. We can see that there is a good correlation between $\beta_{1,4}$ and SpO_2. Tests 1, 2 and 3 had a correlation coefficient of r = 0.995, 0.980 and 0.990 respectively between $\beta_{1,4}$ and SpO_2.

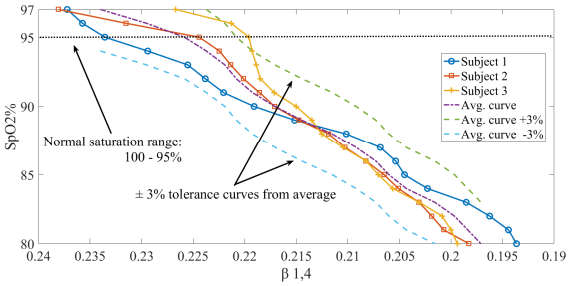

Fig. 15 a. Relation between SpO_2 and $\beta_{1,4}$.

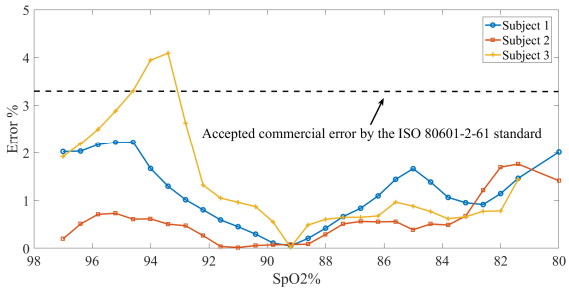

Fig. 15 b. Percentual error curves for the three tests.

7. Discussion – Possible extention to Venous Oxygen Saturation Estimation

Oxygen saturation in the peripheral venous blood (SvO_2) also has physiological and clinical significance, as it enables an evaluation of the severity of shock or cardiac failure [23]. Its estimation by optical means was already reported by changing the venous blood volume with the application of a handcuff to the patient's hands and fingers. It permitted to calculate the absorption difference between a "relaxed" state and a "pressured" state. As done in classic pulse oximetry calculations, a ratio between two wavelengths in the "relaxed" and "pressured" state was obtained to estimate venous saturation. In contrast to arterial saturation, there is no accepted method for the SvO_2 estimation [3].

With our methodology, we consider we can estimate SvO_2 without occlusion. Indeed, the nonpulsatile portion of the plethysmogram represents all the other components met by the light beam all along its optical path including the venous blood. Assuming nail, skin and bone absorptions remain

constant, an estimation of the SvO_2 might also be made by relating the change in the "equivalent wavelength" seen by the BQJ, with the DC component of the PPG.

8. Conclusion

A novel method for estimating blood oxygen saturation has been introduced. For the first time, a multispectral photodiode has been utilised to estimate SpO_2 with a single led. Two of the three in-vivo results from the SpO_2 estimations fall within the accepted tolerance range of 3%, and among the others, a maximum error of 4% was found in the third one. Our estimations were solely calculated with the change in absorption between channels. So, precision and robustness can be increased by adding some of the already developed correction algorithms regularly used to fix common oximetry sources of errors such as motion artifacts [11]. It is worth stressing that only two of the four channels were used for this implementation. This is because it is preferable to use channels with highest and opposite sensitivity for the chosen wavelength. However, other wavelengths can be used for exploiting the other two channels. For instance, the estimation of other types of hemoglobins (e.g. carboxyhemoglobin and methemoglobin) or other physiological parameters.

The proposed approach can also be complementary to the classic or the multiwavelength pulse oximetry approach, as long as the BQJ is employed as the photodetector. Additionally, with this new methodology, we can quantify the changes through the whole finger, including venous blood, so a venous oxygen saturation technique might be developed in the future.

Additionally, a study regarding the influence of skin color and nail polish will be performed, as we estimate that the use of one led could reduce the errors introduced by an increased melanin or the presence of nail polish.

At the end, the proposed system is fully compatible with a monolithic integration for the development of future connected objects targeting well-being applications.

Acknowledgments

We would like to thank to Mr. Guo-Neng Lu, Mr. P. Pittet, Mr. T. Courcier and V. Amiez for the access to the BQJ technologies and sensor. We would also like to thank SENACYT, Panama for partial funding of this research.

References

[1] S. Haymond, R. Carriapa, C.S. Eby and M.G. Scott, "Laboratory Assessment of Oxygenation in Methemoglobinemia", Clinical Chemistry, vol. 51, i. 2, pp. 434-444, 2005.

[2] M. Cannesson, C. Besnard, P. Durand, J. Bohé and D. Jacques, "Relation between respiratory variations in pulse oximetry plethysmographic waveform amplitude and arterial pulse pressure in ventilated patients", Critical Care, v. 9, i. 5, pp.562, 2005.

[3] M. Nitzan and H. Taitelbaum, "The measurement of oxygen saturation in arterial and venous blood", IEEE Instrumentation & Measurement Magazine, vol. 11, no. 3, pp. 9-15, 2008.

[4] Schnapp LM, Cohen NH. Pulse oximetry. Uses and abuses. Chest. 1990. Nov;98(5):1244-50. Review.

[5] M. Nitzan, A. Romem and R. Koppel, "Pulse oximetry: fundamentals and technology update", Medical Devices: Evidence and Research, p. 231, 2014.

[6] J. Schmitt, "Simple photon diffusion analysis of the effects of multiple scattering on pulse oximetry", IEEE Transactions on Biomedical Engineering, vol. 38, no. 12, pp. 1194-1203, 1991.

[7] Nitzan, M., Noach, S., Tobal, E., Adar, Y., Miller, Y., Shalom, E. and Engelberg, S. (2014). Calibration-Free Pulse Oximetry Based on Two Wavelengths in the Infrared — A Preliminary Study. Sensors, 14(4), pp.7420-7434.

[8] Q. Milner and G. Mathews, "An assessment of the accuracy of pulse oximeters", Anaesthesia, vol. 67, no. 4, pp. 396-401, 2012.

[9] S. J. Barker, J. Curry, D. Redford and S. Morgan, "Measurement of carboxyhemoglobin and methemoglobin by pulse oximetry: a human volunteer study", Anesthesiology, vol. 105, no. 5, pp. 892-897, 2006.

[10] G. J. Kost and N.K. Tran, "Continuous noninvasive hemoglobin monitoring: the standard of care and future impact", Crit Care Med, vol. 39, no. 10, pp. 1-6, 2011.

[11] J. M. Goldman, M. T. Petterson, R. J. Kopotic, S J. Barker, "Masimo Signal Extraction Pulse Oximetry", Journal of Clinical Monitoring and Computing, vol. 16, pp. 475-483, 2000.

[12] M. Theodor, D. Ruh, S. Subramanian, et al., "Implantable pulse oximetry on subcutaneous tissue", IEEE International Conference of the Engineering in Medicine and Biology Society (EMBC), pp. 2089-2092, 2014.

[13] S. F. LeBoeuf, H. Zhang, J.F. Muth, R. Splinter and A.T. Finle, "Custom multi-wavelength monolithic optical source applied to sensing of physiological and biometrical parameters",

IEEE International Conference on High Capacity Optical Networks and Enabling Technologies (HONET), pp. 202-206, 2012.

[14] S. Dong, S. Duan, Q. Yang, J. Zhang, G. Li and Renyi Tao, "MEMS based Smart Gas Metering for Internet of Things", IEEE Internet of Things Journal, pp. 1-8, 2017.

[15] G. N. Lu, M.B. Chouikha, G. Sou and M. Sedjil, "Colour detection using a buried double p-n junction structure implemented in the CMOS process", Electronic Letters, vol. 32, ino. 6, p. 594-596, 1996.

[16] S. Feruglio, V.F. Hanna, G. Alquie, G. Vasilescu, "Dark Current and Signal-to-Noise Ratio in BDJ Image Sensors", IEEE Transactions on Instrumentation and Measurement, vol. 55, I. 6, pp. 1892-1903, 2006.

[17] S. Feruglio, F. Haned, G. Vasilescu, M.B. Chouikha, G. Sou, V.F. Hanna, G. Alquie, "A general model of the CMOS buried double junction photodetector", in proceeding of IEEE International Workshop on Imaging Systems and Techniques, pp. 60-65, 2004.

[18] M. B. Chouikha, G.N. Lu, M. Sedjil, G. Sou and G. Alquie, "Buried triple p-n junction structure in a BiCMOS technology for color detection", in proceedings of the Bipolar/BiCMOS Circuits and Technology Meeting, pp. 108-111, 1997.

[19] S. Feruglio, T. Courcier, O. Tsiakaka, et. al., "A CMOS Buried Quad p-n Junction Photodetector Model", IEEE Sensors Journal, vol. 16, no. 6, pp. 1611-1620, 2016

[20] C. Richard, T. Courcier, P. Pittet, S. Martel, L. Ouellet, GN. Lu, V. Aimez and P.G. Charette, "A CMOS Buried Quad p-n Junction Photodetector Model", OPTICS EXPRESS Journal, vol. 20, no. 3, pp. 2053-2061, 2012.

[21] Thierry Courcier. Développement d'un dispositif intégré de photodétection de grande sensibilité avec discrimination spectrale pour les laboratoires sur puce. Optique [physics.optics]. Université Claude Bernard - Lyon I, 2014.

[22] Omlc.ogi.edu. (2017). Tabulated Molar Extinction Coefficient for Hemoglobin in Water. [online] Available at: http://omlc.ogi.edu/spectra/hemoglobin/summary.html [Accessed 1 Dec. 2017].

[23] Ousmane, M., LeBuffe, G. and Vallet, B. Utilisation de la SvO2. Réanimation, 12(2), pp.109-116, 2003.

[24] M. Nitzan, A. Babchenko, B. Khanokh and H. Taitelbaum, "Measurement of oxygen saturation in venous blood by dynamic near infrared spectroscopy", Journal of Biomedical Optics, vol. 5, ino. 2, pp. 155, 2000.